# Development of a pulsed, variable-energy positron beam for atomic scale defect studies

A. C. L. Jones, 1, 2, a) R. G. Greaves, C. L. Codding, and F. A. Selim<sup>1, 2</sup>

(Dated: 23 February 2022)

Positron annihilation spectroscopy provides a sensitive means of non-destructive characterization of materials, capable of probing single atom vacancies in solids with  $10^{-7}$  sensitivity. We detail here the development of a magnetically guided, variable energy, pulsed positron beam designed to conduct depth-dependent defect studies in metals, semiconductors, and dielectrics which will be the first of its kind in the US. The design of the target stage provides capabilities for measurements during  $in\ situ$  annealing up to  $800^\circ$  C and incorporates a new approach to minimize the background due to energetic backscattered positrons. The developed beam at Bowling Green State University provides a powerful tool for characterization of thin films, devices, and ion irradiated materials.

# I. INTRODUCTION

Atomic scale defects, such as single or few atom vacancies, are virtually unavoidable in any macroscopic material. Depending on the application, their presence can be either desirable or detrimental. Defects can arise through a number of different pathways<sup>1</sup>. For example, they can be created during the growth of a material, or they can occur due to the presence of contaminants or dopants. They can also be created via thermal excitation or irradiation. Defects also play an important role in the mechanisms of many interactions and phenomena in materials such as diffusion<sup>2</sup>. Understanding the production, distribution, and dynamics of atomic scale defects is crucial for a broad range of applications, from thin film and solid state devices to the development of high-strength materials for the next generation of nuclear reactors.

Following thermalization, positrons implanted into a material typically diffuse over a range on the order of  $\sim 100$  nm. Defects can trap the positrons leading to characteristic changes in the positron annihilation parameters. Thus positrons provide a uniquely sensitive probe of atomic scale defects via positron annihilation spectroscopy (PAS)^{3-5}. Positron annihilation lifetime spectroscopy (PALS) can provide a sensitive measure of defect size and concentration down to the scale of single atom vacancies, a regime not readily accessible to high resolution transmission electron microscopy, while coincident Doppler spectroscopy can illuminate the chemical environment at the annihilation site. For a detailed review about PAS see Refs.  $^{5-7}$ .

In order to conduct positron annihilation lifetime spectroscopy in metals, oxides and many other systems, where typical observed positron lifetimes lie in the range

of 100-500 ps<sup>7-10</sup>, it is necessary to achieve a comparable time resolution. Conventionally such studies <sup>11-16</sup> have employed direct deposition of <sup>22</sup>Na on the sample or sandwiched a <sup>22</sup>Na source between two identical samples and measured the time interval between detection of a 1.27 MeV  $\gamma$  emitted as a positron is produced and one of the 511 keV  $\gamma$ s produced upon annihilation. However, due to the broad energy spectrum of positron emission from <sup>22</sup>Na, implantation depths vary from just a few nm up to  $\sim$  1 mm, thus such systems are limited to studies of bulk properties. Using a pulsed beam and varying the beam energy it is possible to control the positrons mean implantation depth and perform depth resolved PALS to investigate ion-induced defects, which are often limited to micron depths.

#### II. THE BEAMLINE

There are a variety of techniques for producing and controlling positrons<sup>17</sup>. Positrons can be produced via nuclear interactions or pair production. The most commonly used source of positrons is the radioactive decay of <sup>22</sup>Na due to its 2.6 year half-life, however at present the flux of these Na based beams is limited by the 50 mCi sources commercially available to  $\lesssim 10^7$  slow positrons per second. Systems employing pair-production sources can yield beams with 1-2 orders of magnitude higher flux<sup>18,19</sup>. Regardless, few facilities have been successful in developing a pulsed beam with a time resolution suitable for studies of condensed matter systems<sup>20–26</sup>, with the first depth resolved PALS measurements in ionirradiated metals only being collected recently<sup>27</sup>. From all sources the energy distribution of emitted positrons is quite broad - the mean energy of a positron emitted via  $^{22}$ Na decay is  $\sim 220$  keV, with a full width at halfmaximum (FWHM) energy spread of  $\sim 260 \text{ keV}^{28,29}$ . In order to achieve fine control of the beam energy, the

<sup>&</sup>lt;sup>1)</sup> Department of Physics and Astronomy, Bowling Green State University, Bowling Green, OH 43402, USA

<sup>&</sup>lt;sup>2)</sup>Center for Photochemical Sciences, Bowling Green State University, Bowling Green, OH 43402, USA

<sup>&</sup>lt;sup>3)</sup> 344 Via Colinas, Thousand Oaks, CA 91362, USA

<sup>&</sup>lt;sup>a)</sup>Corresponding author: adricj@bgsu.edu

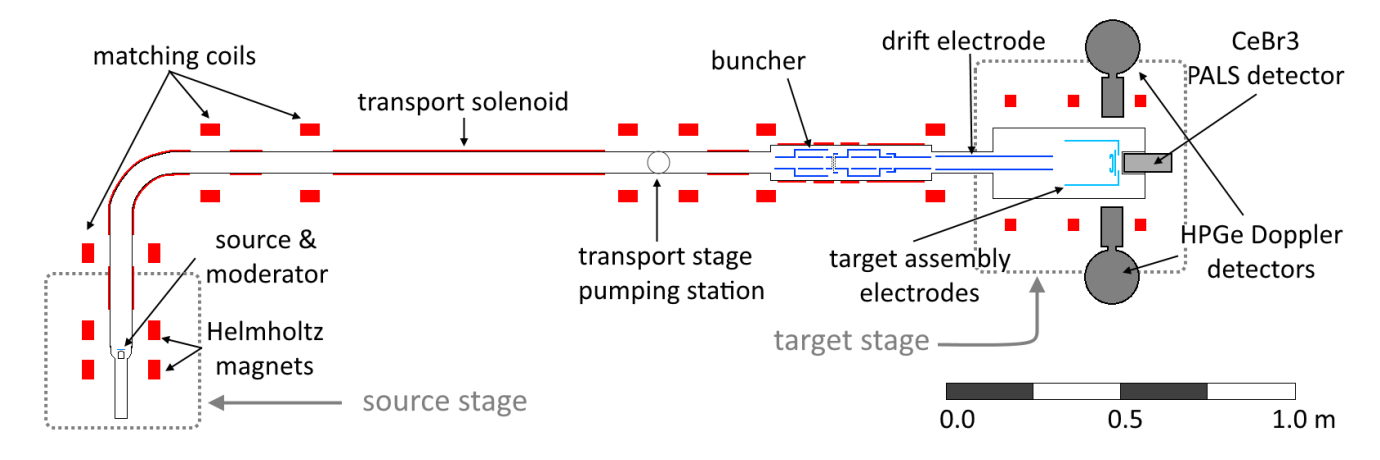


FIG. 1. Simplified schematic overview of the positron beamline illustrating the system from the source chamber through to the target chamber. Transport magnets are shown in red, electrodes in the buncher and target stage are blue and detectors are grey.

positrons must go through a process of moderation. The most common moderation materials are solid neon<sup>30</sup> or thin metal foil moderators<sup>31</sup>. In both examples energetic positrons are stopped within the material and diffuse to the surface. In metal foil moderators positrons that thermalize near a surface may be ejected by the negative work function of the material. In rare-gas moderators positrons rapidly cool until they reach the band gap: positrons reaching the surface with sufficient energy to overcome the work function are emitted $^{32}$ . Due to the long diffusion length of slow positrons in neon it exhibits the highest moderation efficiency, with systems reporting moderated beam intensities representing about  $0.5\%^{33,34}$ of the initial activity and an energy spread of around 1.5 eV FWHM<sup>35,36</sup>. The most commonly used foils are single crystal tungsten or nickel; here the efficiency is typically 1-2 orders of magnitude lower than the solid neon moderators, but the energy distribution can be more than five times narrower<sup>37</sup>. Due to the comparatively broad energy spread, neon moderated systems typically employ buffer gas traps to capture and cool the moderated beam, producing a pulsed beam with an approximately thermal energy distribution, but with a trapping efficiency of  $\sim 20\%^{38,39}$ 

Once positrons have been moderated the beam can be manipulated using electric and magnetic fields. Purely electrostatic beams offer some flexibility in focusing a beam on a target and can be easier to extract to field free regions for sensitive measurements, but typically have lower transport efficiencies than magnetically guided beams<sup>40</sup> and target illumination can depend strongly on beam energy<sup>41</sup>. In this beam, magnetic fields are used to axially confine the beam, while static potentials are used to adiabatically control the axial energy of the beam. Use of time-varied potentials provides a means of differentially accelerating the beam and thus allows us to convert the DC moderated beam into a pulsed beam.

We describe here the design of a W foil-moderated

slow positron beam intended for depth controlled atomicscale defect studies. A schematic overview of the beamline is given in Fig. 1, detailing the outline of the vacuum chamber, the positioning of the source capsule and moderator foil, the magnetic transport coil arrangement, the buncher and target stage electrode structures and the PAS detection setup for both Doppler and PALS measurements. The beamline can be described in three stages: 1) a source stage which houses the <sup>22</sup>Na source and moderator foil, 2) a transport and bunching stage which moves the DC slow positron beam away from the source chamber (necessary to reduce the observed background of  $1.27~\mathrm{MeV}$  and  $511~\mathrm{keV}$  gammas due to  $^{22}\mathrm{Na}$ decay and positron annihilation that is not fully attenuated by the source chamber shielding) and converts it into a pulsed beam of sub-ns bunches, and 3) a target stage housing a biased target assembly, allowing for depth resolved Doppler spectroscopy and annihilation lifetime spectroscopy measurements. We also describe the design of a separate moderator annealing chamber which, with the use of a removable vacuum assembly, allows for the routine transfer and annealing and conditioning of moderator foils under UHV conditions, with observed pressures in the system typically in the low  $10^{-9}$  Torr range.

Elements of the system have been simulated in this work, either to optimize the design or guide experiments. The results presented here are primarily from Monte Carlo simulations of charged particle trajectories applying the Lorentz force and were prepared entirely in Matlab. Particle trajectories are propagated through a 4th order Runge-Kutta approximation<sup>42</sup>. Electric fields were calculated using Matlab's PDE toolbox or via iterative relaxation, while magnetic fields were calculated as the sum of sets of single current loops for which complete analytic solutions exist<sup>43</sup>.

#### 1. Source stage

The arrangement of shielding material and the source loading procedure / mechanism implemented in the source stage illustrated in Fig. 2 is based on the solid-neon moderated source stages produced by First Point Scientific<sup>44</sup>, however the use of a foil moderator introduces the need that the foil be mounted on a manipulator system so that it can be removed from the source chamber for annealing.

A sealed <sup>22</sup>Na source is seated inside a tungsten assembly, mounted inside a custom four-way cross vacuum chamber. The activity of the source was recorded as  $\sim$  5 mCi in November 2019 and was calculated to be  $\sim 3.7$  mCi at installation. It should be noted that the source was originally intended for a polarized beam and features a low-Z backing material, slightly reducing the expected beam yield. The beamline vacuum system is primarily constructed from DN63CF fittings, though the rear port of the source chamber and the removable moderator vacuum suitcase, are DN40CF. The tungsten assembly provides both radiation shielding and ensures close alignment of the source and moderator foil assembly. The chamber is situated inside of an aluminum canister with an internal diameter of 305 mm that is filled with lead shot. Additional shielding plugs fill the rear nipple, one tungsten (nearest the source) and one stainless steel. A small spring positioned between the rear plug and the sealing flange provides about 10 N of force to prevent the source from shifting. A long tungsten plug with a central 19 mm aperture is placed in the outgoing nipple, corresponding to a solid angle of about 1 part in 640 at the exit aperture of the plug. This limits the emission of high energy unmoderated positrons to about 0.16 % of the source activity, however for energies  $\lesssim 10 \text{ keV}$  the magnetic field is sufficient to confine an increasingly larger fraction of the positrons with cyclotron radii smaller than the aperture in the shielding. The vacuum pumping system and pressure gauges are mounted beneath the table. Shielding is provided by two partially trimmed cylinders 64 mm long each with an inset cutaway on their mating surfaces providing a channel for pumping. The shields are mounted in opposition such that there is no direct line of sight to the source. An offaxis pin ensures the shielding plugs remain in alignment.

The tungsten assembly that houses the source and controls the spacing and alignment of the moderator with the source was designed to maximize the efficiency of positron flux on the moderator. This design was based on simulation of the basic geometry of the source and foil. It is assumed that the source is evenly distributed at the base of a small cup ( $\sim 0.5$  mm deep) and only positrons emitted in a forward direction are considered. Backscattered positrons are neglected, while positrons colliding with the source cup walls are considered lost. Simulated collection efficiency results are plotted in Fig. 3 for moderator foils 8.5 and 11 mm in diameter, comparable to the unobstructed surface areas using either the 10 mm

single crystal or 15 mm polycrystalline foil moderators. Due to the line of sight obstruction of the cup that the source is deposited in there is practically no advantage to setting the moderator closer than  $\sim 2$  mm.

Throughout the beamline positrons are guided by an axial magnetic field. In the source canister a pair of magnetic coils, wound on 159 mm diameter forms, are positioned either side of the chamber, in a nearly Helmholtz configuration ( $\Delta z \sim 1.3 \times r$ ). A solenoid is wound on the outgoing nipple, arranged to minimize variation in the field amplitude. Pairs of rectangular correction coils are also attached to ensure axial alignment of the moderated beam while they traverse the tungsten shielding plug. This nipple is encased in cast lead shields which extend outside of the shielding canister, supported and contained by a 152 mm diameter pipe extending about 76 mm out from the canister.

# 2. Moderator assembly

The moderator assembly detailed in Fig. 4 is mounted from above the source chamber, on the end of a linear manipulator with 610 mm travel (NorCal MLR-275-050-24). A pair of manual gate valves separated by a short reducing tee allow for the moderator assembly to be retracted from the source chamber. Both chambers are then sealed and the assembly is removed under vacuum for annealing. An aluminum structure, mounted internally on the zero length adapter flange (DN63CF-DN35CF) at the top of the source chamber, positions and supports the tungsten source assembly. Between the posts of this support structure, blocks with channels that widen upwards provide a rail system that guides the moderator assembly into place in the tungsten source assembly, an important feature given the rotational freedom provided by the magnetically coupled linear manipulator. To allow the guiding rail to correct any misalignment of the moderator assembly, in the direction of the beam axis at least, the mounting structure that couples the moderator assembly to the linear manipulator is made from 0.75 mm stainless steel shim stock that can be deflected with a small force.

The moderated beam is accelerated axially by a repulsive potential applied to the moderator foil, delivered via a 0.125 mm tungsten wire that is pinned in place with the foil. The wire is runs out of the moderator assembly through an inset insulated alumina tube as depicted. A second insulating tube fixes the wire in place between the assembly and the stainless steel support above. Above the flexible support, a connection is made to a kapton insulated wire lead that is loosely wound around the linear manipulator up to a BNC feedthrough on the removable moderator vacuum chamber assembly. Typically the beam energy is set at  $\leq 30$  eV, though the electrical isolation of the foil (which is held between two half-bisque ceramic washers) likely permits application of a few hundred volts. Low energy is preferred here to minimize non-adiabatic transport, particularly as the beam is first

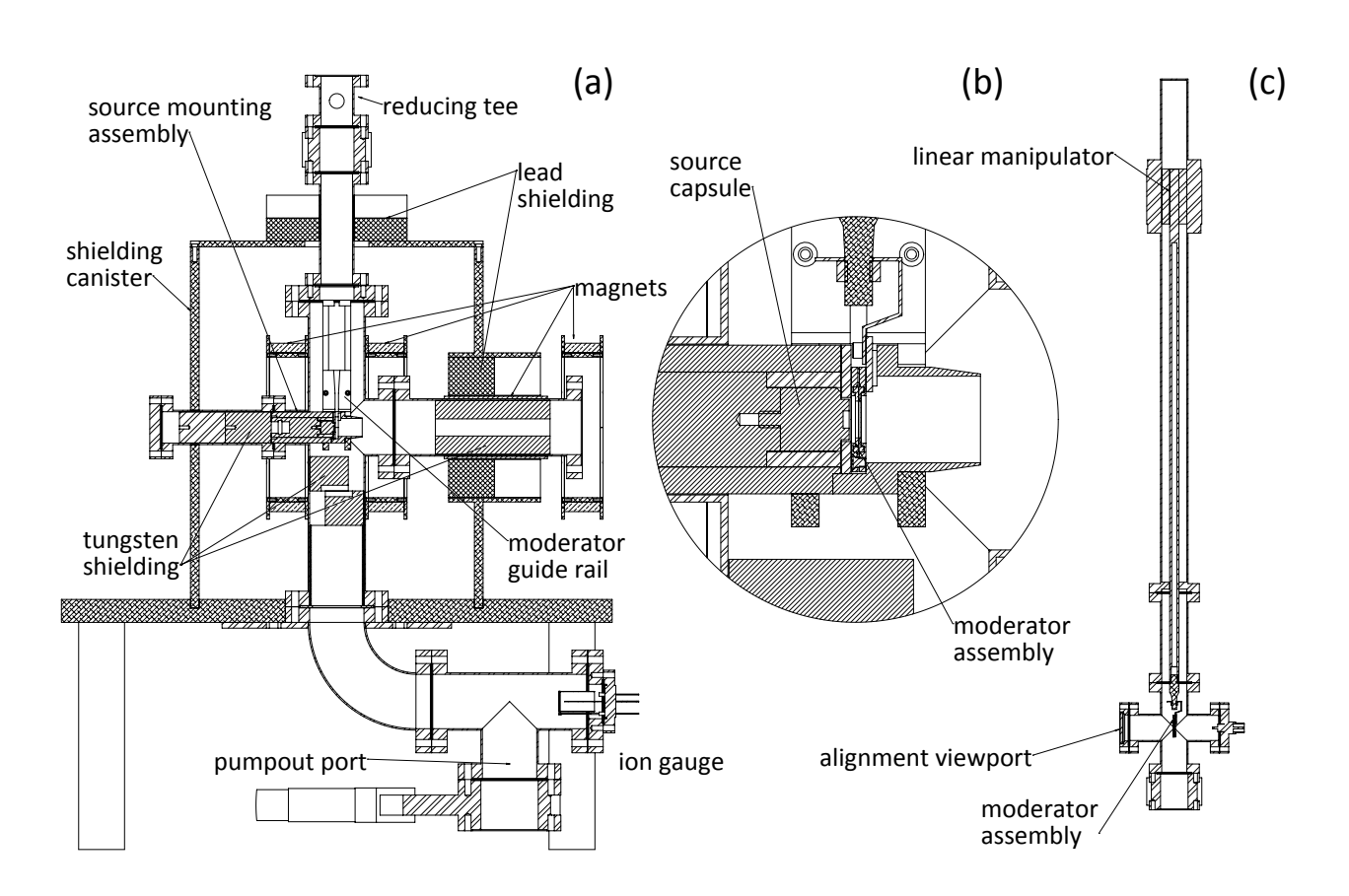


FIG. 2. Figure (a) is a cross section view of the source stage illustrating the source & moderator mounting and alignment structures, and the arrangement of radiation shielding, excluding the lead shot that fills the cannister. (b) is an expanded view of the source assembly with the moderator assembly installed. The removable moderator vacuum assembly is illustrated in (c) and includes a linear manipulator, viewport for alignment of the assembly prior to installation, and a BNC feedthrough used to apply a bias to the moderator foil that defines the beam's transport energy. Different shading indicates material type.

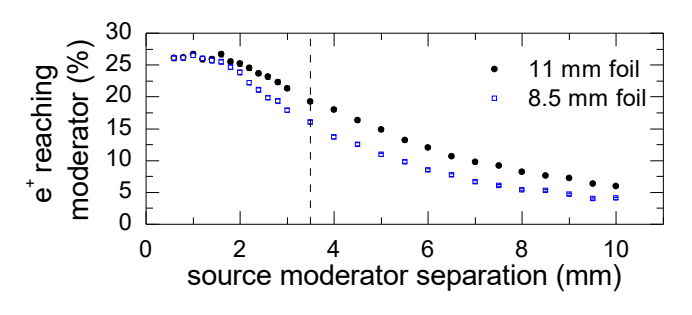


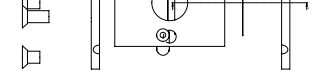
FIG. 3. Simulated percentage of positrons reaching the moderator foil as a function of the separation of the source and moderator. The dashed vertical line indicates the separation achieved in the apparatus.

accelerated, and makes operation of the RF bunching system simpler. The accelerating electric field is defined across the gap between the foil and a 70% transmitting high-purity tungsten mesh. The mesh is woven high-purity tungsten, chosen to minimize the risk of contam-

ination of the moderator foil under annealing. As the mesh lies just  $\sim 0.5$  mm from the moderator, the mesh spacing selected was the smallest commercially available choice in order to minimize any radial fringe field due to leakage through the mesh.

# 3. Transport

The guiding magnetic field is set at a nominal magnitude of 100 Gauss. The primary guiding magnets are all wound from enamel coated magnet wire with a rectangular cross section measuring  $2.9\times1.3$  mm. Matching coils, wound on 159 mm ID forms, are mounted as needed at flanges. Both the number of layers of each matching coil and the lengths and positions of each solenoid have been calculated to minimize variations in the axial field strength throughout the transport line, ensuring adiabatic transport of the moderated beam  $^{45}$ . Solenoids are wound directly onto the vacuum nipples and are typically



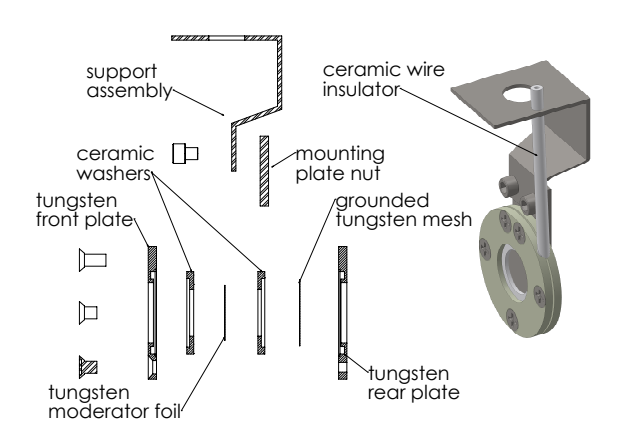


FIG. 4. Detail of the moderator assembly. An exploded cross section of the assembly illustrating the individiual components is illustrated on the left. The moderator foil is pressed between two half-bisque ceramic washers which seat into grooves in the tungsten plates of the assembly. A 70% transmitting tungsten wire mesh is spot welded to the inner rim of the rear plate, approximately 0.5 mm from the foil. A thin tungsten wire is held against the foil and provides the bias that controls the beam transport energy. The assembled structure is depicted in color on the right side of the figure. The hooked stainless steel support assembly is bolted to the base of the linear manipulators central rod via a threaded rod adapter which is not shown here.

constructed with two layers of windings.

To minimize background contributions from the source stage, positrons are transported through a path length of over 2 meters prior to bunching and implantation at the target. Immediately following the source stage there is a 90° elbow with a 152 mm bending radius. This places the target chamber out of direct line of sight of the source and acts as a crude velocity filter, with simulation indicating a cutoff in the transmission of positrons above  $\sim 1.5~\rm keV$  as illustrated in Fig. 5 plot (a). For the moderated beam the non-uniform field density across the bend results in a deflection along the axis perpendicular to the plane of the bend. Simulation indicates a deflection of  $5.04\pm0.02~\rm mm$ , in good agreement with the post-bend correction field applied.

Following the elbow there is a pair of rectangular correction coils that correct the out of plane drift. The two 20 turn coils are folded over the beam tube transport solenoid in a saddle coil arrangement on a straight section of the beamline and measure 127 mm long by 64 mm wide. Following the transport line gate valve there is a longer set of rectangular correction coils, two pairs of 20 turn coils, which provides a gentle correction to the horizontal and vertical position of the beam. An additional set will also be included on the buncher system to ensure axial transport throughout and allow for accurate positioning of the beam on the target.

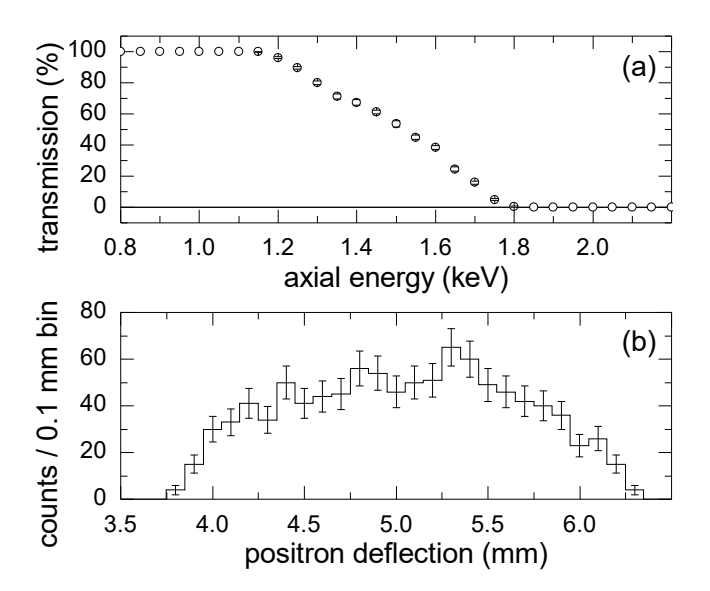


FIG. 5. (a) Simulated transmission efficiency of a magnetically guided 10 mm diameter beam through the  $90^{\circ}$  bend at the exit of the source stage as a function of energy. (b) Distribution of out-of-plane deflection of moderated positrons transmitted through the bend.

#### 4. Buncher

The buncher system is based on the design of Maekawa and Kawasuso<sup>46</sup>. It is composed of three distinct RF driven sections; 1) a prebuncher, 2) a chopper and 3) the main buncher as illustrated in Fig. 6. The buncher system is designed to produce pulses at a rate of 40 MHz, the driving frequency of both the prebuncher and chopper. The main buncher is operated at 80 MHz with pulses bunched across both the entrance and exit gaps. Prebunching the DC beam allows the throughput to be improved as compared to a system with only a single bunching stage.

The electrodes of the buncher are made from OFHC Cu (also known as Cu-101) to ensure minimal resistance. The electrode stack is assembled with electrodes mounted on polytetrafluoroethylene (PTFE) spacers. Both ends are capped with 3 mm 304 stainless plates with bolt hole patterns matching the PTFE spacers. Most of the spacers have an OD closely matching the chamber ID, centering the electrode stack in the chamber. Mounting insulators have multiple additional holes drilled to allow for efficient pumping of the buncher chamber. A set of four stainless steel 8-32 threaded rods are fed through the PTFE spacers and end plates and are fastened with nuts against the end plates. A rectangular cutout along the bottom of the support structure houses an OFHC Cu grounding bar. The grounding bar is screwed to the custom mounting gasket at the entrance of the stack (i.e., the side the positrons enter from). All of the electrodes that hold static potentials are capacitively coupled to the adjacent grounding bar to reduce the amplitude of RF pickup and minimize unwanted heating of the beam.

The driving potential of the RF electrodes is produced via two Siglent arbitrary waveform generator (AWG) units, the prebuncher and chopper, which require only moderate potentials ( $|V| < \pm 30 \text{ V}$ ) and operate at a frequency of  $\sim 40$  MHz, are driven by an AWG 6022x. The prebuncher, which requires the smallest power to operate, is driven directly by the output of the AWG which can output up to 20 Vpp. For the chopper and main buncher the AWG outputs (Channel 2 of the 6022x for the chopper and Channel 1 of a Siglent AWG 6052x for the main buncher) are first amplified, through mini-circuits ZHL-2-S+ and ZHL-03-5WF+ units respectively. The amplified signal is then coupled through to the buncher via RF resonator units, tuned to the required frequencies of  $\sim 40$  and 80 MHz. The main buncher, driven at double the fundamental bunching frequency, is operated such that the bunch is accelerated across both gaps.

In order to minimize the RF power requirements for bunching, helical resonators are installed on the chopper and buncher electrodes. The design is based on the considerations outlined by Deng *et al.*<sup>47</sup>. Because the chopper and buncher electrode capacitances heavily load the resonators, the final design parameters were tuned empirically using a vector network analyzer (AURSINC NanoVNA V3.4) to obtain optimal performance.

The resonators consist of a helical copper winding enclosed in a cylindrical copper cavity 7.5 cm in diameter and 10 cm long. The coils are 2.0 cm in diameter and are wound from 3 mm diameter copper wire. For the 80 MHz unit, the resonator coil consists of 3.25 turns with a 1.5 cm pitch, while the 40 MHz coil has 5.8 turns with 0.95 cm pitch. The RF signal is coupled inductively to the 80 MHz and 40 MHz resonators using primaries consisting of 1.5 and 3.5 turns, respectively. The Q-factors of the resonators, measured using a vector network analyzer, are 121 and 98, respectively.

#### 5. Target stage

The target chamber was designed to accommodate several needs. It must provide access for the detectors, support high voltages for positron implantation and minimize background contributions to the signal. At the implantation energies of interest to our intended experiments a significant fraction of the incident positrons can be backscattered; for example  $\sim 15\%$  of positrons incident on an Fe target at energies between 10 to 30 keV are backscattered and this fraction increases with increasing target atomic number Z, reaching  $\sim 40\%$  for Au<sup>48–50</sup>. Without mitigation efforts, these backscattered positrons would return to the sample at a later time and may ruin the timing structure of the pulsed beam. In a similar magnetically guided beam, backscattered positrons were prevented from returning to the target through the use of an  $E \times B$  deflector<sup>24</sup>. As the time range of interest for our intended atomic defect studies is  $0 \le t \lessapprox 2$  ns, it is sufficient to delay the recapture of the reflected positrons.

The target chamber, illustrated in Fig. 7 houses a removable target assembly, mounted on the rear DN200CF flange of the chamber. The assembly is enclosed within a large cylinder which is biased to the same potential as the target (though could be isolated and independently biased if needed), this serves to delay the return of backscattered positrons such that they are not detected in the time window relevant for PALS measurements.

The bulk of the chamber and target assembly is made from 304 stainless steel, while electrical isolation and support is achieved with ceramic standoffs and PTFE supports. A pair of high-power 30 kV feedthroughs provide the target bias and allow for target heating through a resistance wire mounted to the target between the upper assembly that houses the target and a thin mounting plate seated  $\sim 5$  mm behind it, separated by small ceramic standoffs. This system is driven via a biased DC supply that it is powered through an isolation transformer (Stangenes SIT 50-1000). Using 30 $\Omega/\mathrm{ft}$  resistance wire, a total heating power of  $\sim 90$  W should be achievable with a 3 A driving current. Estimation of the radiative heat losses at 800° C yields a power requirement of about 87 W.

The target is mounted at the base of a 12.7 cm diameter cylinder which is biased to the same potential as the target. This creates a region of minimal electric field which allows the backscattered positrons to drift over a region of  $\sim 10$  cm before reflecting near the open end of the cylinder. The chamber has a 20 cm diameter, which allows the target and associated assembly to support a bias of up to  $\sim 30$  kV, providing depth dependent implantation to  $\sim 1 \, \mu \text{m}$  or higher. Under testing the target stage has been successfully biased to -27 kV. Tests were performed at a base pressure of  $\sim 10^{-9}$  Torr, with the voltage ramped up over  $\sim 10$  minutes. When minor discharges occurred the supply voltage was backed off a small amount then held constant for about a minute to condition the assembly. Improvements made to the internal electrical connection following the first tests had no impact on the achievable limit. The most likely cause of breakdown is field emission from the front opening of the HV canister, which has the sharpest features in the target assembly.

Backscattering from the target has been simulated to estimate its impact on the PALS time structure. Simulated positron reflection times are plotted in Fig. 8. Fig. 8 (a) is a stacked histogram of reflection times at a 30 keV implantation energy, distinguishing annihilation on the HV can from positrons returning to the target. The dashed vertical line indicates the upper limit of the typical measurement time window. At 30 keV signal within the 0-2 ns time range is dominated by annihilation on the can, which can be easily screened. Annihilation on the can at a much greater mean separation from the PALS detector and is thus naturally attenuated, however this signal can also be further reduced by placing the detector behind a lead or tungsten aperture. In Fig. 8 (b) distributions are shown for positrons return-

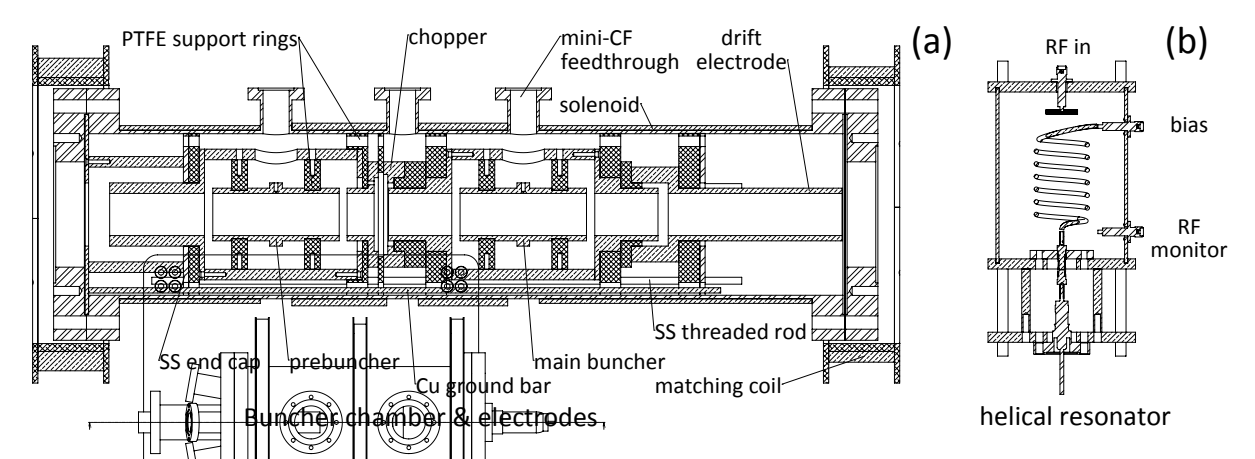
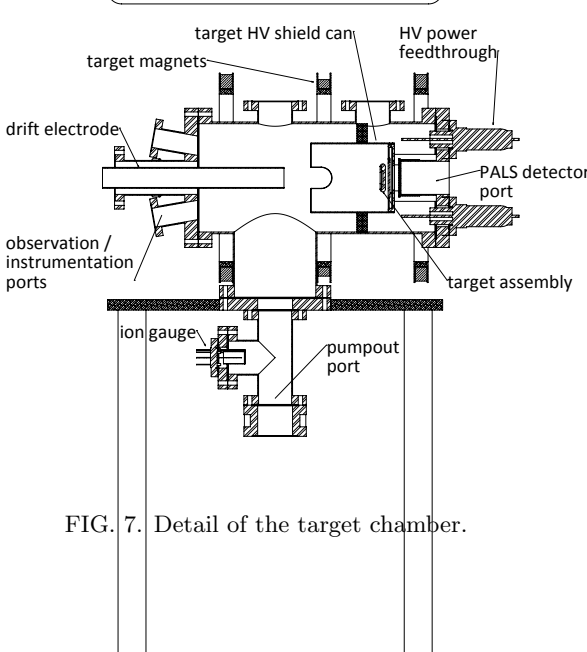


FIG. 6. (a) Detail of the buncher electrode assembly, vacuum chamber, and magnet system. (b) Helical resonator assembly used to deliver the RF power to the chopper and main buncher electrodes. The two resonators need to be kept on resonance at frequencies of  $\sim 40$  and 80 MHz respectively.



ing to the target only, at simulated implantation energies of 5, 15, and 30 keV. As the positron energy is reduced the return flight time increases. In Fig. 9 the percentage of backscattered positrons returning in the measurement time window (0-2 ns) is plotted as a function of implantation energy. With the geometry of our target stage design there is a maximum in the background signal in the energy range of 2-3 keV. Below 3 keV the late edge of the distribution begins to exceed 25 ns flight time. Due to the 40 MHz bunching cycle, detection times can only be resolved in 25 ns increments, and so the background is shifted back into the detection window. To mitigate this issue, we consider a couple of potential solutions: 1) applying an independent bias to the HV can to shift the energy range of the problem region during measurement of the 2 to 3 keV range or, 2) splitting the HV can into two independent electrodes, allowing us to adjust the effective length of the low-field drift region.

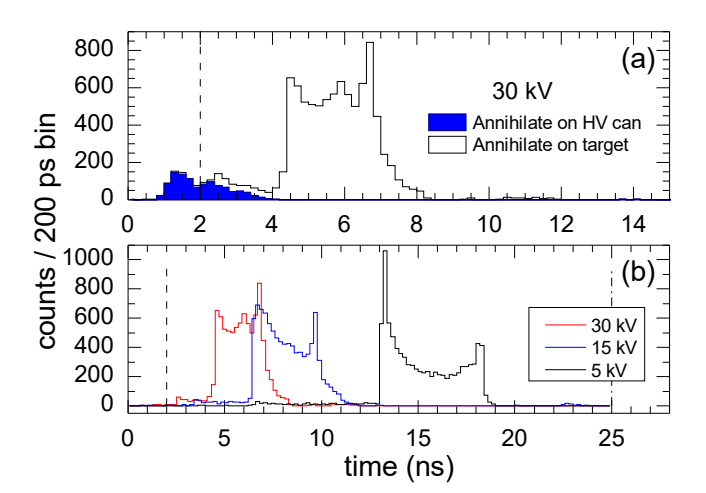


FIG. 8. (a) Simulated time of flight spectra for backscattered positrons implanted at 30 keV. The dark shaded curve represents positrons that annihilate on the HV canister that surrounds the target assembly. A dashed vertical line at 2 ns indicates the upper bound of the time range of interest in defect studies. (b) Time of flight spectra for backscattered positrons returning to the target for implantation energies of 30, 15 and 5 keV (i.e., excluding those positrons that terminate on the HV can, which represent  $\lessapprox 15\%$  of the backscattered positrons). The dash-dotted vertical line at 25 ns indicates one bunching cycle. As individual positron arrival times are unknown, annihilation times can only be determined relative to one duration of the RF cycle.

#### 6. Moderator annealing

Without preparation under UHV conditions moderating foils exhibit poor efficiency and energy distribution. If exposed to air the surface oxide layer inhibits slow positron emission and the observed beam is largely comprised of positrons that are not stopped within the foil, though we have observed a moderated beam from an an-

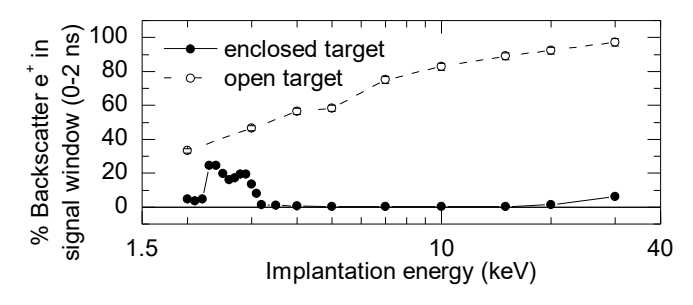


FIG. 9. Percentage of the backscattered positrons returning to the target within the time range of 0-2 ns for a bare target and a target enclosed in a canister at the same potential. Across the full energy range the background signal seen in the enclosed geometry is substantially reduced. Due to the 40 MHz cycle of the bunching system, flight times can only be resolved within a 25 ns time window, so at energies between 2-3 keV the delayed peak becomes prominent due to the typical return flight time exceeding 25 ns. Positron backscattering probabilities fall off at energies below 10 keV.

nealed single-crystal W foil that had subsequently been exposed to air with an intensity  $\sim 1.5\%$  of the typical beam strength. In our beam, due to the weak guiding field in the elbow the background of fast positrons is limited to axial energies  $<1.5~\rm keV,$  and thus represents only a small fraction of the source activity.

Annealing of the W moderator requires heating the foil to a maximum temperature of  $\sim 2100^{\circ}$  C. The annealing chamber illustrated in Fig. 10 is not directly attached to the beamline due to space limitations and out of concern for potential damage to the source capsule. In our annealing scheme heating is achieved by bombarding the foil with a 10 keV electron beam from a high-current gun (Kimball Physics model EGG-3103A with a 50 mA beam current limit). We follow the procedure outlined by the Trento group<sup>37</sup> which involves a staged increase in foil temperature, culminating in a flash heating to the maximum temperature, followed by a gradual cool down period to minimize stress in the annealed foil. Foil temperature is monitored by an externally mounted IR sensor (Optris CTLaser 1MH1) which monitors 1  $\mu$ m radiation, for which the emissivity from W is relatively static as a function of temperature, and operates at T > 800°C.

After a few annealing cycles the foil is allowed to cool to near room temperature, then the moderator assembly is retracted into the vacuum suitcase and sealed off from the annealing chamber. Once the gate valve is closed the ion gauge is switched off and given a couple of minutes to cool. The turbo is then switched off and the backflow valve is operated to stop the turbo, using an Agilent 84 FS turbopump this takes about 10-15 minutes. After the turbo stops the rough pump is switched off and the chamber is slowly backfilled. The sealed vacuum chamber containing the moderator is then removed from the chamber and transferred to the source chamber. Once attached the air-filled reducing tee between the gate valves is roughed out by bleeding the gas through a line attached

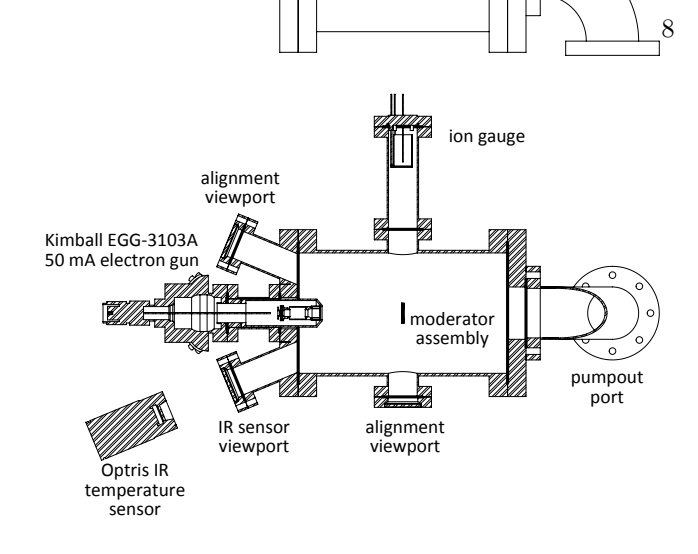


FIG. 10. Detail of the moderator annealing chamber.

to the source rough pump, a process that takes about 20 minutes. After the tee has reached rough pressure, the backing line is closed and the manual gate valve between the tee and the source chamber is carefully opened to leak the remaining gas through the chamber. Here the leak rate is controlled to keep the pressure in the chamber below  $\sim 20~\mu \rm Torr.$  Pumping the tee out to UHV pressure can take a further 1-1.5 hours. The broad energy spread of the moderated beam reported here is likely a result of surface contamination of the moderator foil during transfer. This will be rectified with the installation of a 10 L/s ion pump on the transfer vacuum assembly in the near future.

# III. BEAM CHARACTERISTICS

Two different moderators have been tested in the source stage and the subsequent beams have been examined to determine the beam intensity and energy distribution. The first tests were carried out with a 3  $\mu$ m polycrystalline foil with an 11 mm diameter exposed surface facing the source capsule. The measured resolution was substantially broader than expected. The resolution of the cutoff, estimated from the 12-88% amplitude interval of the cutoff curve (equivalent to the FWHM in a Gaussian distribution), was 2.18 eV. The beam intensity was measured on the target via the count rate detected at the chamber wall, perpendicular to the target assembly, using an unshielded NaI detector. The measured signal rate was  $19.04 \pm 0.80$  counts per second; a simulation of the expected detection efficiency of the experimental arrangement used indicates an extrapolated moderated beam intensity of  $2370 \pm 110$  positrons per second. The measured intensity corresponds to a moderation efficiency of just  $(1.73 \pm 0.08) \times 10^{-5}$ , an order of magnitude lower than anticipated, however the NaI detector signal was essentially terminated when the detector was aligned with the target magnetic field, so some suppression of the

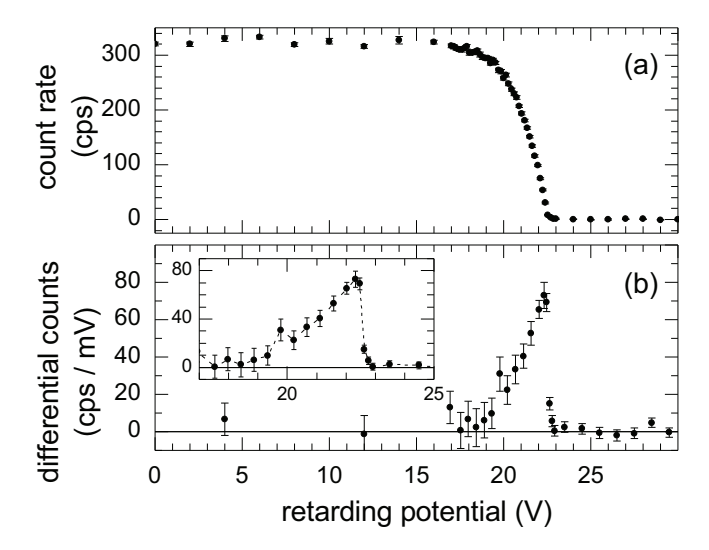


FIG. 11. (a) A background subtracted cutoff curve of the moderated beam from an annealed single-crystal W(100) foil measured at the exit of the buncher system using a  $CeBr_3$  detector and retarding the beam with the first buncher electrode. (b) A differential of the cutoff curve, illustrating the energy distribution. The inset shows an expanded view about the peak of the distribution. Despite the unexpectedly broad resolution, the bias toward low energy makes it possible to work with a narrower resolution by retarding the slow positrons.

signal may have occurred in these measurements.

Following the polycrystalline foil measurements a smaller, single-crystal W(100) foil was installed for the preliminary testing of the bunching system. A typical cutoff curve, with a moderator bias of 20 V is plotted in Fig. 11 plot (a). The beam was cutoff using the drift electrode (see Fig. 6) at the end of the buncher stack (which has the longest aspect ratio of the buncher electrodes) with the beam intensity measured using a magnetically shielded CeBr<sub>3</sub> detector placed next to the blank gasket that terminated the buncher (i.e., with no target chamber present). Here the beam's observed energy distribution was even broader than that from the polycrystalline foil, with a 12-88% interval of 2.8 eV. Fig. 11 plot (b) illustrates the energy distribution, found by differentiating the cutoff curve in plot (a), which is a strongly asymmetric curve with a broad low energy tail. Thus, despite the poor resolution of the moderated beam, it is possible to work with a narrower resolution by retarding the slowest moderated positrons.

The intensity of the single-crystal moderated beam was measured with the CeBr3 detector by looking at the signal at the end of the buncher assembly terminated with a blank Cu gasket. We observed a signal rate of  $227.7 \pm 3.4$  cps. Simulation of the experimental arrangement yields a detection efficiency of  $2.13 \pm 0.05\%$ . Accounting additionally for the missed counts in the Compton spectrum and transmission losses in the buncher (which contains three 90 % transmitting meshes), yields

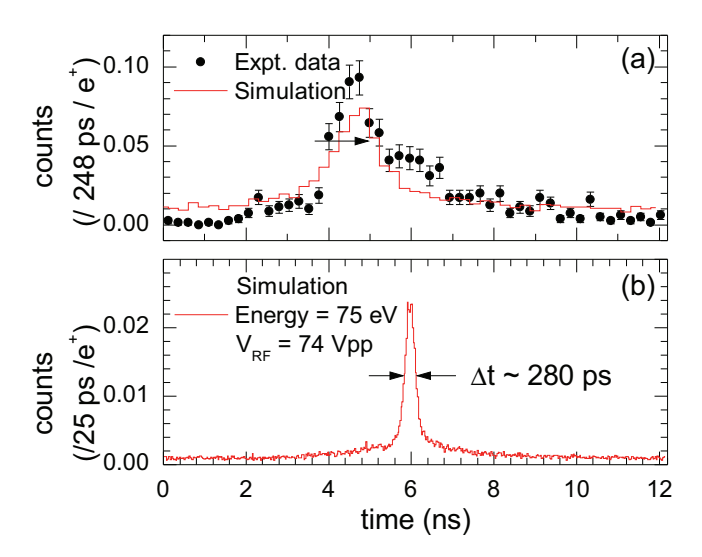


FIG. 12. (a) Data collected operating only the main buncher with a 46 Vpp RF delivered to the resonator and a mean beam energy of  $\sim 56$  eV and a 550 meV FWHM energy spread, compared with a simulated curve at 55 eV beam energy and 0.5 eV FWHM spread and 46 Vpp applied RF. (b) Simulated buncher performance near the optimal achievable settings and an assumed beam energy spread of 300 meV FWHM.

a beam strength of  $18000 \pm 500$  positrons per second. These measurements were made with a source activity of  $\sim 2.83$  mCi, implying a moderation efficiency of  $1.9 \times 10^{-4}$ , near the lower end of the expected range of performance.

Preliminary tests of the buncher utilized only the main buncher and surrounding electrodes. The beam was monitored at the exit of the buncher, which was terminated with a blank Cu gasket. A CeBr<sub>3</sub> detector was mounted inside a lead housing with the scintillator mounted perpendicular to the axis of the beamline. The resonance frequency of the resonator and main buncher system was measured between each test run and found to be relatively stable throughout around  $82.24 \pm 0.04$  MHz. The beam resolution was narrowed by retarding the low energy positrons with the first electrode of the buncher, with an applied potential of +21.8 V rejecting about 2/3of the positrons. The energy of the beam was set by biasing the main buncher and surrounding electrode to -34 V such that transport across the RF electrode took 1.5 cycles, 18.2 ns here, with a mean beam energy of  $\sim 56$  eV. The bunch time resolution was measured for a range of input RF amplitudes, between 0.7 to 1.5 Vpp. The measured output of the amplifier increases Vpp by a factor of  $\sim 42$ , while the on resonance reflection was typically measured at around -20 dB, a 1% attenuation of the power driving the buncher, although larger losses can result from drift in the resonant frequency of the system during the course of experiments.

In Fig. 12 plot (a) data illustrating the experimental performance of the buncher, operated with RF applied only to the main buncher, is compared with a 1D sim-

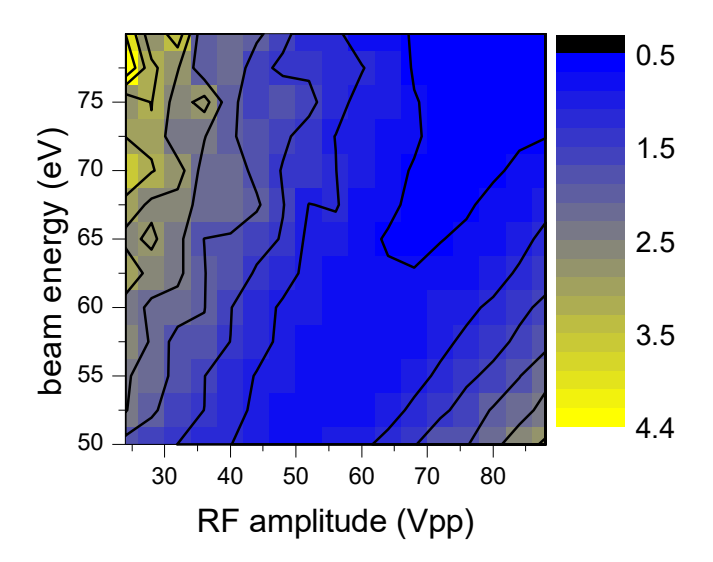


FIG. 13. Simulated bunching performance as a function beam energy through the main buncher and applied RF amplitude. The conditions simulated here closely match the experimental arrangement used for testing the buncher, using only the main buncher and subsequent drift electrode and terminating at the exit of the buncher. Due to the varying time distribution of the bunches it was not possible to fit a consistent function to the simulated data, so time resolution reported is found by subtracting a linear background from the data and finding the time width that encompasses 12-88% of the pulse area which represents the FWHM of a Gaussian distribution.

ulation of comparable settings. In this simulation, all positrons are confined to the axis, which allowed the simulated electric field to be accurately modeled as a sum of Gaussians. The experimental data is well described by a sum of two independent Gaussians, a narrow bunched pulse on a broad background. A fit to the data indicates that the narrow pulse width is about  $920 \pm 110$  ps and accounts for  $\sim 28\%$  of the positrons. The simulated data has a significantly broader, nearly uniform background, however the FWHM of the bunch is comparable and accounts for  $\sim 30\%$  of the positrons. The best resolution observed in our preliminary experiments was 880±140 ps, applying a 1.0 Vpp input, corresponding to an RF amplitude of  $\sim 42$  Vpp, however this should only be considered an upper bound of the performance as there is significant broadening arising from the experimental setup used to test the operation of the buncher. A simulated bunch time distribution is plotted in Fig. 12 (b), operating at close to the maximum achievable RF amplitude and assuming a beam energy spread of 300 meV FWHM. The calculated time resolution achieved under these conditions is  $280 \pm 10$  ps.

Simulated bunching results are plotted in Fig. 13 applying conditions as similar as possible to the experimental bunching arrangement tested. Pulsed time resolution is determined as a function of the mean incident beam energy in the main buncher and the applied peak-to-peak RF voltage. Due to variation in the shape of bunched

pulses across the parameter space explored it was not feasible to fit a consistent model to each pulse shape to extract the time resolution. An estimate of the bunched time resolution was made by first subtracting the background from the signal, then converting the remaining curve into a cumulative distribution function and finding the time interval encompassing 12 to 88% of the signal, which yields the FWHM for a Gaussian distribution. There is a clear line of optimal performance. By chance this occurs where the applied RF amplitude Vpp is approximately equal to the mean beam energy in eV through the main buncher. All of the experiments so far were conducted with a mean beam energy of  $\sim 56~{\rm eV},$  so further improvements in the time resolution should be readily achievable.

#### IV. SUMMARY

The first <sup>22</sup>Na based pulsed positron beam with subnanosecond timing resolution in the US was developed to provide a depth resolved probe for atomic scale defects through PALS and coincident Doppler broadening spectroscopy. The source stage design combines elements of existing solid-neon moderator based systems and foil moderator systems. A novel approach is introduced to overcome the contribution of backscattered positrons that are recaptured by the attractive potential of the target and would otherwise overlap with the pulse time structure and thus interfere with PALS measurements. The chamber and target assembly are designed to allow in-situ annealing up to 800°C providing for measurements of thermal populations of defects. Additionally, a new design for moderator annealing and transfer was introduced to enable efficient moderator annealing to be undertaken in a separate chamber away from the radioactive source, minimizing the risk of damaging the source capsule. This newly developed beam provides a powerful tool for defect measurements in metals and oxides which will advance studies of ion irradiated materials and development of high-strength radiation-resistant materials. It also provides a highly desirable probe for thin films, semiconductors, and multilayer devices.

#### **ACKNOWLEDGMENTS**

We would like to thank Prof. Allen Mills for valuable insights throughout the development of the beamline. Work was supported as part of FUTURE (Fundamental Understanding of Transport Under Reactor Extremes), an Energy Frontier Research Center funded by the U.S. Department of Energy (DOE), Office of Science, Basic Energy Sciences (BES) and in part by the National Science Foundation (NSF) under Award # DMR-2005064.6

#### **AUTHORS' CONTRIBUTIONS**

A.C.L.J designed the apparatus, performed simulations and prepared the manuscript. C.L.C contributed to the design and machining of many components. R.G.G. assisted in the design of the buncher system and designed the resonators and associated electronics. F.A.S. was the PI of the project and contributed to the design of the system and preparation of the manuscript.

#### **DATA AVAILABILITY**

The data that support the findings of this study are available from the corresponding author upon reasonable request.

# **CONFLICT OF INTEREST**

The authors have no conflicts to disclose.

- <sup>1</sup>C. Freysoldt, B. Grabowski, T. Hickel, J. Neugebauer, G. Kresse, A. Janotti, C. G. Van de Walle, First-principles calculations for point defects in solids, Rev. Mod. Phys. 86 (2014) 253. doi: 10.1103/RevModPhys.86.253.
- URL https://doi.org/10.1103/RevModPhys.86.253
- <sup>2</sup>G. S. Collins, X. Jiang, J. P. Bevington, F. A. Selim, M. O. Zacate, Change of diffusion mechanism with lattice parameter in the series of lanthanide indides having l1<sub>2</sub> structure, Phys. Rev. Lett. 102 (2009) 155901. doi:10.1103/PhysRevLett.102.155901. URL https://doi.org/10.1103/PhysRevLett.102.155901
- <sup>3</sup> J. Čížek, Characterization of lattice defects in metallic materials by positron annihilation spectroscopy: A review, J. Mater. Sci. Technol. 34 (2018) 577–598. doi:10.1016/j.jmst.2017.11.050. URL https://doi.org/10.1016/j.jmst.2017.11.050
- <sup>4</sup>V. Slugeň, S. Sojak, W. Egger, V. Krsjak, J. S. Veternikova, M. Petriska, Radiation damage of reactor pressure vessel steels studied by positron annihilation spectroscopy - a review, Metals 10 (2020) 1378. doi:10.3390/met10101378.
- URL https://doi.org/10.3390/met10101378
- <sup>5</sup>F. A. Selim, Positron annihilation spectroscopy of defects in nuclear and irradiated materials a review, Mater. Charact. 174 (2021) 110952. doi:10.1016/j.matchar.2021.110952.
- URL https://doi.org/10.1016/j.matchar.2021.110952
- <sup>6</sup>P. Asoka-Kumar, M. Alatalo, V. J. Ghosh, A. C. Kruseman, B. Nielsen, K. G. Lynn, Increased elemental specificity of positron annihilation spectra, Phys. Rev. Lett. 77 (1996) 2097. doi:10.1103/PhysRevLett.77.2097.
- $_{
  m URL}$  https://doi.org/10.1103/PhysRevLett.77.2097
- <sup>7</sup>P. Hautojärvi (Ed.), Positrons in solids, Springer, 1979. doi: 10.1007/978-3-642-8136-0.
- <sup>8</sup>P. A. Sterne, J. H. Kaiser, First-principles calculations of positron lifetimes in solids, Phys. Rev. B 43 (1991) 13892. doi:10.1103/PhysRevB.43.13892.
- URL https://doi.org/10.1103/PhysRevB.43.13892
- <sup>9</sup>M. Masataka, A. Hideki, S. Yashuaru, Theoretical calculations of positron lifetimes for metal oxides, Mater. Trans. 45 (2004) 1964–1967. doi:10.2320/matertrans.45.1964.
- $\operatorname{URL}\ \mathtt{https://doi.org/10.2320/matertrans.45.1964}$
- <sup>10</sup> J. M. Campillo Robles, E. Ogando, F. Plazaola, Positron lifetime calculation for the elements of the periodic table, J. Phys. Condens. Matter 19 (2007) 176222. doi:10.1088/0953-8984/19/17/ 176222
  - ${\rm URL\ https://doi.org/10.1088/0953\text{--}8984/19/17/176222}$

- <sup>11</sup>R. Krause-Rehberg, H. S. Leipner, Positron annihilation in semiconductors: defect studies, Springer, 1999.
- <sup>12</sup>M. Eldrup, Positron methods for the study of defects in bulk materials, J. Phys., IV 5 (1995) C1-93. doi:10.1051/jp4:1995111. URL https://doi.org/10.1051/jp4:1995111
- <sup>13</sup>H. E. Schaefer, R. Gugelmeier, M. Schmolz, A. Seeger, Positron lifetime spectroscopy and trapping at vacancies in aluminum, Mater. Sci. Forum 15 (1987) 111–116. doi:10.4028/www.scientific.net/MSF.15-18.111.
- URL https://doi.org/10.4028/www.scientific.net/MSF.
- <sup>14</sup>A. Kawasuso, M. Hasegawa, M. Suezawa, S. Yamaguchi, K. Sumino, An annealing study of defects induced by electron irradiation of Czochralski-grown Si using a positron lifetime technique, Appl. Surf. Sci. 85 (1995) 280–286. doi:10.1016/0169-4332(94) 00344-0.
  - URL https://doi.org/10.1016/0169-4332(94)00344-0
- <sup>15</sup>F. A. Selim, D. Winarski, C. R. Varney, M. C. Tarun, J. Ji, M. D. McCluskey, Generation and characterization of point defects in SrTio<sub>3</sub> and Y<sub>3</sub>Al<sub>5</sub>O<sub>12</sub>, Results Phys. 5 (2015) 28–31. doi:10.1016/j.rinp.2015.01.002.
  - URL https://doi.org/10.1016/j.rinp.2015.01.002
- <sup>16</sup>K. Saarinen, P. Hautojärvi, P. Lanki, C. Corbel, Ionization levels of As vacancies in as-grown GaAs studied by positronlifetime spectroscopy, Phys. Rev. B 44 (1991) 10585. doi: 10.1103/PhysRevB.44.10585.
- URL https://doi.org/10.1103/PhysRevB.44.10585
- 17C. Hugenschmidt, Positrons in surface physics, Surf. Sci. Rep. 71
   (2016) 547-594. doi:10.1016/j.surfrep.2016.09.002.
   URL https://doi.org/10.1016/j.surfrep.2016.09.002
- <sup>18</sup>R. Krause-Rehberg, S. Sachert, G. Brauer, A. Rogov, K. Noack, EPOS - An intense positron beam project at the ELBE radiation source in Rossendorf, Appl. Surf. Sci. 252 (2006) 3106–3110. doi: 10.1016/j.apsusc.2005.08.109.
- URL https://doi.org/10.1016/j.apsusc.2005.08.109
- <sup>19</sup>C. Hugenschmidt, G. Kögel, R. Repper, K. Schreckenbach, P. Sperr, B. Strasser, W. Triftshäuser, Intense positron source at the munich research reactor frm-ii, Appl. Phys. A 74 (2002) s295–s297. doi:10.1007/s003390201398.
- URL https://doi.org/10.1007/s003390201398
- <sup>20</sup>N. Alberola, A. T., C. Badertscher, A. Bas, A. S. Belov, P. Crivelli, S. N. Gninenko, N. A. Golubev, M. M. Kirsanov, A. Rubbia, D. Sillou, Development of a high-efficiency pulsed slow positron beam for measurements with orthopositronium in vacuum, Nucl. Instrum. Methods Phys. Res. A 560 (2006) 224–232. doi:10.1016/j.nima.2006.01.025.
  - URL https://doi.org/10.1016/j.nima.2006.01.025
- <sup>21</sup>W. Egger, P. Sperr, G. Kögel, G. Dollinger, Pulsed low energy positron system (pleps) at the munich research reactor frm ii, Phys. Status Solidi c 4 (2007) 3969–3972. doi:10.1002/pssc. 200675812.
- URL https://doi.org/10.1002/pssc.200675812
- <sup>22</sup>C. Hugenschmidt, B. Löwe, J. Mayer, C. Piochacz, P. Pikart, R. Repper, M. Stadlbauer, K. Schreckenbach, Unprecedented intensity of a low-energy positron beam, Nucl. Instrum. Methods Phys. Res. A 593 (2008) 616–618. doi:10.1016/j.nima.2008.05.038.
  - $\mathrm{URL}\ \mathtt{https://doi.org/10.1016/j.nima.2008.05.038}$
- <sup>23</sup>N. Oshima, R. Suzuki, T. Ohdaira, A. Kinomura, T. Narumi, A. Uedono, M. Fujinami, Rapid three-dimensional imaging of defect distributions using a high-intensity positron microbeam, Appl. Phys. Lett. 94 (2009) 194104. doi:10.1063/1.3137188. URL https://doi.org/10.1063/1.3137188
- <sup>24</sup>J. P. Sullivan, J. Roberts, R. W. Weed, M. R. Went, D. S. Newman, S. J. Buckman, A trap-based positron beamline for the study of materials, Meas. Sci. Technol. 21 (2010) 085702. doi:10.1088/0957-0233/21/8/085702.
- URL https://doi.org/10.1088/0957-0233/21/8/085702
- $^{25}{\rm N.}$  Djourelov, D. Dinescu, V. Leca, An overview of the design of elips a new slow positron beam line, Nucl. Instrum. Methods

- Phys. Res. A 934 (2019) 19-25. doi:10.1016/j.nima.2019.04.032.
- URL https://doi.org/10.1016/j.nima.2019.04.032
- <sup>26</sup>J. R. Machacek, S. McTaggart, L. W. Burggraf, Single-shot positron annihilation lifetime spectroscopy using a liquid scintillator, AIP Advances 11 (2021) 055223. doi:10.1063/5.0048366. URL https://doi.org/10.1063/5.0048366
- <sup>27</sup>S. Agarwal, M. O. Liedke, A. C. L. Jones, E. Reed, A. A. Kohnert, B. P. Uberuaga, Y. Q. Wang, J. Cooper, D. Kaoumi, N. Li, R. Auguste, P. Hosemann, L. Capolungo, D. J. Edwards, M. Butterling, E. Hirschmann, A. Wagner, F. A. Selim, A new mechanism for void-cascade interaction from non-destructive depth-resolved atomic-scale measurements of ion irradiation-induced defects in Fe, Sci. Adv. 6 (2020) aba8437. doi:10.1126/sciadv.aba8437.
  - URL https://doi.org/10.1126/sciadv.aba8437
- <sup>28</sup>B. T. Wright, Spectrometer measurement on the high energy positrons of sodium 22, Phys. Rev. 90 (1953) 159. doi:10.1103/ PhysRev.90.159.2.
- $\mathrm{URL}\ \mathtt{https://doi.org/10.1103/PhysRev.90.159.2}$
- <sup>29</sup>G. R. Massoumi, P. J. Schultz, W. N. Lennard, J. Ociepa, Positron emission yields for encapsulated <sup>22</sup>na sources, Nucl. Instrum. Methods Phys. Res. B 30 (1987) 592–597. doi:10.1016/ 0168-583X(88)90136-X.
- URL https://doi.org/10.1016/0168-583X(88)90136-X
- <sup>30</sup>A. P. Mills Jr., E. M. Gullikson, Solid neon moderator for producing slow positrons, Appl. Phys. Lett. 49 (1986) 1121. doi:10.1063/1.97441.
- URL https://doi.org/10.1063/1.97441
- <sup>31</sup>A. P. Mills Jr., P. M. Platzman, B. L. Brown, Slow-positron emission from metal surfaces, Phys. Rev. Lett. 41 (1978) 1076. doi:10.1103/PhysRevLett.41.1076.
- URL https://doi.org/10.1103/PhysRevLett.41.1076
- <sup>32</sup>E. M. Gullikson, A. P. Mills Jr., Positron dynamics in rare-gas solids, Phys. Rev. Lett. 57 (3) (1986) 376.
- <sup>33</sup>N. Oshima, T. M. Kojima, D. Dumitriu, A. Mohri, H. Oyama, T. Kambara, Y. Kanai, Y. Nakai, M. Wada, Y. Yamazaki, Development of a slow-positron source, Phys. Rev. Lett. 57 (1986) 276.
- <sup>34</sup>R. Khatri, M. Charlton, P. Sferlazzo, K. G. Lynn, A. P. Mills Jr., L. O. Roellig, Improvement of rare-gas solid moderators by using conical geometry, Appl. Phys. Lett. 57 (1990) 2374. doi: 10.1063/1.103856.
  - URL https://doi.org/10.1063/1.103856
- <sup>35</sup>R. G. Greaves, C. M. Surko, Solid neon moderator for positron-trapping experiments, Can. J. Phys. 74 (1996) 445–448. doi: 10.1139/p96-063.
  - URL https://doi.org/10.1139/p96-063
- <sup>36</sup>S. Ghosh, J. R. Danielson, C. M. Surko, Energy distribution and adiabatic guiding of a solid-neon-moderated positron beam, J. Phys. B.: At. Mol. Opt. Phys. 53 (2020) 085701. doi:10.1088/ 1361-6455/ab7642.
- URL https://doi.org/10.1088/1361-6455/ab7642
- <sup>37</sup>A. Zecca, L. Chiari, A. Sarkar, S. Chattopadhyay, M. J. Brunger, Procedures for conditioning W- and Ni-moderators for application in positron-scattering measurements, Nucl. Instrum. Meth-

- ods Phys. Res. B 268 (2010) 533-536. doi:10.1016/j.nimb. 2009.11.013.
- URL https://doi.org/10.1016/j.nimb.2009.11.013
- <sup>38</sup>J. Clarke, D. P. van der Werf, B. Griffiths, D. C. S. Beddows, M. Charlton, H. H. Telle, P. R. Watkeys, Design and operation of a two-stage positron accumulator, Rev. Sci. Instrum. 77 (2006) 063302. doi:10.1063/1.2206561.
  - ${\rm URL}\ {\tt https://doi.org/10.1063/1.2206561}$
- <sup>39</sup>D. B. Cassidy, S. H. M. Deng, R. G. Greaves, A. P. Mills Jr., Accumulator for the production of intense positron pulses, Rev. Sci. Instrum. 77 (2006) 073106. doi:10.1063/1.97441. URL https://doi.org/10.1063/1.97441
- <sup>40</sup>A. Zecca, Positron beam development and design, Appl. Surf. Sci. 194 (2002) 4–12. doi:10.1016/S0169-4332(02)00099-5.
- ${\rm URL\ https://doi.org/10.1016/S0169\text{--}4332(02)00099\text{--}5}$
- A. Zecca, M. Bettonte, J. Paridaens, G. P. Karwasz, R. S. Brusa,
   A new electrostatic positron beam for surface studies, Meas. Sci.
   Technol. 9 (1998) 409-416. doi:10.1088/0957-0233/9/3/014.
   URL https://doi.org/10.1088/0957-0233/9/3/014
- <sup>42</sup>D. Tan, C. Zheng, On a general formula of fourth order rungekutta method, J. Math. Sci. Math. Ed. 7 (2012) 1–10.
- <sup>43</sup>J. Simpson, J. Lane, C. Immer, R. Youngquist, Simple analytic expressions for the magnetic field of a circular current loop, NASA technical documents (2001).
- <sup>44</sup>C. M. Surko, S. J. Gilbert, R. G. Greaves, Non-Neutral Plasma Physics III, RL Spencer, and RC Davidson (American Institute of Physics, New York), 1999, edited by J. J. Bollinger.
- <sup>45</sup>J. A. Young, C. M. Surko, Charged particle motion in spatially varying electric and magnetic fields, Nucl. Instrum. Methods Phys. Res. B 247 (2006) 147–154. doi:10.1016/j.nimb.2006. 01.052.
  - URL https://doi.org/10.1016/j.nimb.2006.01.052
- <sup>46</sup>M. Maekawa, A. Kawasuso, Development of pulsed positron beam line with compact pulsing system, Nucl. Instrum. Methods Phys. Res. B 270 (2012) 23–27. doi:10.1016/j.nimb.2011. 10.001.
- URL https://doi.org/10.1016/j.nimb.2011.10.001
- <sup>47</sup>K. Deng, Y. L. Sun, W. H. Yuan, Z. T. Xu, J. Zhang, Z. H. Lu, J. Luo, A modified model of helical resonator with predictable loaded resonant frequency and q-factor, Rev. Sci. Instrum. 85 (2014) 104706. doi:10.1063/1.4897478.
  - URL https://doi.org/10.1063/1.4897478
- <sup>48</sup>P. G. Coleman, L. Albrecht, K. O. Jensen, A. B. Walker, Positron backscattering from elemental solids, J. Phys.: Condens. Matter 4 (1992) 10311–10322. doi:10.1088/0953-8984/4/50/018.
- URL https://doi.org/10.1088/0953-8984/4/50/018

  49 J. Mäkinen, S. Palko, J. Martikainen, P. Hautojärvi, Positron
- backscattering probabilities from solid surfaces at 2-30 kev, J. Phys.: Condens. Matter 4 (1992) L503–L508. doi:10.1088/0953-8984/4/36/006.
- URL https://doi.org/10.1088/0953-8984/4/36/006
- <sup>50</sup>G. R. Massoumi, W. N. Lennard, P. J. Schultz, A. B. Walker, K. O. Jensen, Electron and positron backscattering in the medium-energy range, Phys. Rev. B 47 (1993) 11007–11018. doi:10.1103/PhysRevB.47.11007.
  - URL https://doi.org/10.1103/PhysRevB.47.11007